Adaptative Friction Shock Absorbers and Reverse Thrust for Fast Multirotor Landing on Inclined Surfaces

John Bass, Isaac Tunney, and Alexis Lussier Desbiens

***Abstract*—Small multirotors are not capable of landing in complex situations, such as on inclined surfaces, in wind gusts or at high impact velocities. This paper explores the use of lightweight friction shock absorbers, combined with rapid thrust reversal, to increase the landing envelope of a quadrotor. The friction shock absorbers serve to dissipate the drone's kinetic energy and the reverse thrust increases the maximum slope inclination at which it can land. A landing gear prototype was designed and implemented on a DJI F450, and a model was created to generate landing maps to evaluate its benefits. Finally, the technology was tested in real outdoor conditions. The overall system enables drones to safely land on surfaces of up to 60° and at vertical speeds of up to 2.75 m/s, thus increasing the landing envelope by a factor of 8, compared to traditional multirotors.**

***Index Terms*—Actuation and joint mechanisms, aerial systems: mechanics and control, dynamics.**

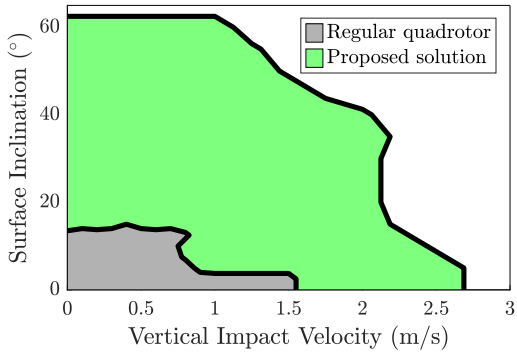

Fig. 1. Landing envelope of a conventional quadrotor [4] vs. a quadrotor equipped with friction shock absorbers and reverse thrust, discussed in this paper. The landing envelope is described as the conditions (surface inclination and vertical impact speed) which permits a safe landing.

I. Introduction

In RECENT years, hardware onboard small uninhabited aerial vehicles (UAVs) has improved, granting them greater capabilities for commercial applications. However, the landing phase of most UAVs remains challenging, as most accidents occur at this moment [1]. The landing envelope of conventional multirotors, shown in Fig. 1, remains limited as they are primarily designed to land on near-horizontal fixed surfaces at low speeds. They are not well suited for landing in complex conditions such as on slanted surfaces or in high winds, which would lead to a failed or aborted landing. As a multirotor tries to land on an inclined surface, it will most likely end up flipping over due to its rigid landing gears and thrust redirection. Furthermore, wind gusts greatly affect the outcome of multirotor landings, even on flat terrain [2]. Multiple applications would benefit from increasing the landing envelopes of such drones. By allowing higher descent and impact speeds during landing, UAVs would be less influenced by external perturbations. Potential applications include landing on uneven and slanted terrains, or landing on roofs for emergency situations [3] or surveillance tasks.

Recently, a variety of platforms have been developed to address the small size of multirotor landing envelopes. Some have proposed the use of dynamic manoeuvres [5], [6] to enable UAVs to quickly approach the desired landing area and rapidly reorient themselves before hitting the surface. While these platforms are able to land on vertical surfaces, they require situational awareness and specialized adhesion mechanisms (e.g., dry-adhesives, micro-spines) to successfully land. The emergence of omnidirectional multirotors [7] has also inspired researchers to install lateral rotors on a quadrotor, allowing it to land at any angle [8]. Articulated motorized landing gears have also been designed to enable small quadrotors to land on inclined and uneven terrain in a slow and controlled manner by adapting their geometry to the surface [9]–[11]. Another approach was to use 3D-printed corrugated shock absorbers to allow a quadrotor to land at vertical speeds of up to 2 m/s on horizontal surfaces [12]. While the cited mechanisms each increase different aspects of multirotor landing envelopes, these improvements come at the cost of substantially increasing empty weight and therefore decreased flight time, as noted in Table I.

In previous work, the authors proposed the use of reverse thrust (RVT) to improve the landing envelope of an unmodified DJI F450 [4]. The quadrotor was able to land on inclined surfaces of up to 25° at vertical impact speeds of up to 1 m/s, but the

Manuscript received February 24, 2022; accepted April 28, 2022. Date of publication May 20, 2022; date of current version May 31, 2022. This letter was recommended for publication by Associate Editor G. Endo and Editor C. Gosselin upon evaluation of the reviewers' comments. This work was supported in part by NSERC Canadian Robotics Network (NCRN), in part by Uninhabited Aircraft Systems Training, Innovation, and Leadership Initiative (UTILI), and in part by the Fonds de recherche du Québec (FRQ). *(John Bass and Isaac Tunney are co-first authors). (Corresponding author: John Bass.)*

The authors are with the Createk Design Lab, 3IT, Université de Sherbrooke, Sherbrooke, QC J1K 2R1, Canada (e-mail: john.bass@usherbrooke.ca; isaac.tunney@usherbrooke.ca; alexis.lussier.desbiens@usherbrooke.ca).

This letter has supplementary downloadable material available at https://doi.org/10.1109/LRA.2022.3176102, provided by the authors.

Digital Object Identifier 10.1109/LRA.2022.3176102

TABLE I
ADVANTAGES AND LIMITS OF RECENT UAV LANDING TECHNOLOGIES

Method	Lateral Rotors[8]	Actuated Landing Gear[10]	Damper Landing Gear[12]	RVT[4]
			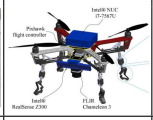	
Angle	30° slopes	30° slopes	Horiz. surface	25° slopes
Vel.	0.5 m/s	0.5 m/s	2 m/s	1 m/s
Mass	Added mass	920 g added	410 g added	None added

stiff and undampened nature of the landing gear limited further improvement.

While the use of reverse thrust has the benefit of being a purely software solution, it is limited by the rotor dynamics and reversal delays (∼250 ms). Indeed, the rotors can not transition fast enough to damp the fast rebounds of traditional landing gears (10-30 ms), causing the UAV to flip over during high velocity and/or steep landings. The design of a lightweight damping landing gear would create optimal conditions to use RVT by extending the impact duration and dissipating most of the system's kinetic energy. This article proposes the use of adjustable friction dampers combined with RVT to allow high velocity landings on steep slopes.

The rest of this paper is structured as follows: Section II describes the benefits of friction dampers and the design strategy chosen to accomplish the task of landing on slanted surfaces, while section III presents a prototype incorporating this technology. A dynamic model, created to evaluate and optimize the performance of the system in a wide range of conditions, is detailed in Section IV. Finally, Sections V and VI present the resulting landing envelopes, complemented with experimental validation in outdoor conditions.

II. LANDING STRATEGY

The main objective of this work is to enable UAVs to land at high impact speeds on steep slopes, therefore filling the void seen in landing performances. Landing at high speeds, which shortens landing duration, has the benefit of reducing the time a UAV can be influenced by external perturbations. As an example, landing at an approach velocity of 3 m/s, starting from 1 m above the surface, would give external perturbations only 0.33 s to exercise their influence. More typical landing velocities of less than 0.5 m/s would require approaches of at least 2 s. Furthermore, a damped landing gear could allow for a wider range of landing conditions, simplify the required control, sensing and computing requirements.

A. Friction Damping

Friction has many potential advantages for use in landing gears:

- Constant dissipative torque: Friction provides a relatively constant force over a given displacement, which in turn can maximise energy dissipation.
- No elastic energy accumulated in the landing gear: Less energy is re-injected into the system, therefore reducing bounces and promoting a constant contact with the ground.
- Design simplicity and relatively low mass compared to traditional oil-based dampers.

A variety of friction-based implementations are available, such as disk brakes. However, friction shock absorbers (FSAs) were chosen as they can be implemented with less mass and parts. FSAs are used to provide damping by pressing disks together to generate friction [13]. Desired friction levels can be obtained by varying the number of friction pads and the compression force.

B. Friction With Reverse Thrust

As mentioned in Section I, previous work [4] has shown that the rotor dynamics are too slow to truly take advantage of RVT when compared to the rapid impacts caused by rigid landing gear. This physical limitation can however be alleviated when RVT is combined with friction shock absorbers. They spread the impact forces over a longer period of time and prevent rebounds, providing enough time for RVT to generate significant downwards thrust and counter any tipping motion of the quadrotor.

C. Adjustable Friction Levels

A friction-based shock absorber will stay in its compressed position after landing. To have the ability to land again after takeoff, the friction shock absorbers should be actuated or allowed to reset themselves by deactivating the friction to let gravity or a weak spring reset the landing gear. This later concept can easily be implemented without adding much mass. A small actuator can vary the compression force on the disks to increase or decrease the friction level. This also allows adjustable friction levels, which can be exploited to allow full compression of the landing gear at different landings speeds.

D. Optimization Variables

To further increase the landing envelope, two variables were targeted for their significant influence on the landing performances.

1) Asymmetric Friction Torques: The downhill legs will impact the ground with higher velocities due to the higher drop height and the angular velocity created during the contact of the uphill leg. Different friction levels between the uphill and downhill sets of legs could be employed to better dampen the quadrotor's motion. Knowing this, the model developed in Section IV can be used to find the ideal friction torques as a function of surface inclination and impact velocity. Logically, the ideal friction should result in a full compression of the legs without them reaching their end-of-travel (EOT).

2) Asymmetric Leg Orientation: On steeper surfaces, fully extended legs will make the uphill legs impact the ground with angles close to 90°. In that case, the impact forces will push through the structure instead of rotating the friction joint to dissipate energy. To improve performance, uphill legs orientation can be decreased as the surface's inclination increases. This solution would diminish the total travel allowed in the joints, but, as noted, the uphill joints have less kinetic energy to dissipate and the friction level could be increased. In the current implementation, to keep the design simple and lightweight, the

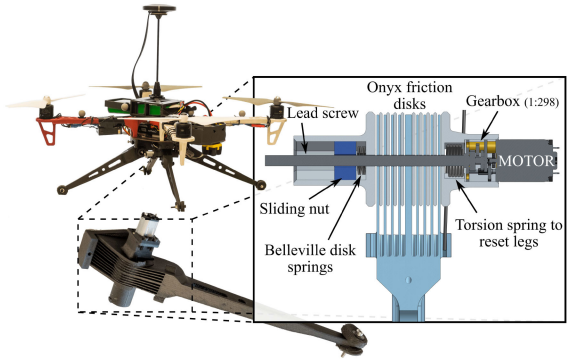

Fig. 2. Close-up view of the landing gear system.

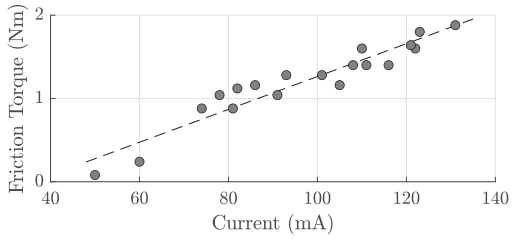

Fig. 3. Measured static friction torque as a function of the motor's current.

legs are not actuated and their angle needs to be manually set before flight.

III. Hardware Implementation

A first prototype of a landing gear incorporating FSAs was 3D-printed and is shown in Fig. 2. The design takes advantage of friction disks that generate friction by rotating relative to one another when the legs get compressed during landing. For each leg, one set of disks is fixed to the base of the drone while the other set is built into the leg. These disks rotate around the lead screw of a small DC motor which controls the level of friction in the joint by adjusting the pressure on the disks. A small torsional spring is incorporated in the joint to reset the leg once loosened. In order to keep the landing gear as light as possible, a high number of disks was chosen. This reduces the torque required by the motor.

The friction joints was sized using an energy method, where the kinetic energy of a 1.55 kg drone travelling at 3 m/s had to be dissipated by four friction shock absorbers, whose work is given by $W = \tau\Delta\theta$. Using a $\Delta\theta$ of 37° and a safety factor of 1.2, a friction torque of 3.2 Nm was required. Trials on a tensile testing machine indicated that the 3D-printing material (Onyx) used provided a friction coefficient of 0.25–0.3. The level of friction torque obtained by compressing disks together is given by [14]:

$$\tau = \frac{2n}{3}\mu_k F_n \left(\frac{{r_o}^3 - {r_i}^3}{{r_o}^2 - {r_i}^2}\right), \tag{1}$$

where n is the number of friction surfaces, μ_k is the kinetic friction coefficient, F_n is the normal force compressing the disks together and r_i and r_o are respectively the inner (3.3 mm) and outer (13 mm) radii of the disks. Knowing that a small 10 g micro DC motors equipped with high reduction ratio gearboxes (1:298) is capable of applying about 75 N through a lead screw, the joints required 18 friction surfaces to create the desired torque. The high reduction ratio allow a reduced total mass, but comes at the cost of lower compression speeds. In this configuration, the motors can set the friction level and reset leg orientation in approximately 10 s.

Current feedback on the motor is used to obtain the desired friction torque for specific landing conditions. The nuts of the lead screw pushes against Belleville disk springs to ensure a more precise control. Fig. 3 presents the measured relation between friction torque and current passing through the motors.

For simplicity reasons, the friction disks and the legs are 3D-printed from only two parts. The material used is Onyx, chosen for its relatively higher strength and capacity to create complex and precise geometries, which is ideal for the thin friction pads (0.8 mm). Lower surface smoothness also allows for more predictable behavior of the friction disks. Other materials could be used in future iteration, including carbon fiber in the leg for added stiffness, as well as materials with higher coefficient of friction in the friction disk.

The total weight of the four friction shock absorbers is 320 g, including the electronics used to control the joint motors, compared to 80 g for the original landing gear. The weight of the proposed system reduces flight time by 16.5% to 14.1 minutes compared to a bare-bones F450. The total mass could eventually be further reduced by using carbon fiber in the legs, smaller/fewer motors, etc.

To ensure more friction between the legs and the landing surface, rubber pads were installed at the feet, providing a static friction coefficient in the range of 1.1 to 1.3 on roofing shingles. Also, in order to fairly compare the performance of the proposed solution to that of traditional landing gears, a similar geometry was employed. This includes similar leg length, leg base, leg count and leg orientation. The friction shock absorbers are also mounted at the same location as the original rigid legs under the base.

Finally, a Pixhawk Cube Orange running Ardupilot is used as the autopilot for the platform. The drone uses standard DJI 2312E motors and DJI 9450 propellers combined with bidirectional ESCs from BLHeli to enable reverse thrust. The limited payload capacity of the F450 quadrotor limits the choice of sensors. Beside the usual sensors (e.g., IMU, barometer, GPS-RTK Here+), a TeraRanger Laser rangefinder was also implemented. The laser rangefinder points downward and is used during landing to tell the autopilot when to stop the motors and start the reverse thrust. With this configuration, the drone weights 1550 g, including the friction landing gear and its electronic system.

IV. Model and Validation

A dynamic model was designed to simulate quadrotor landings at different velocities and on different inclinations. This enables a faster exploration of the landing envelopes, instead of arduously testing all possible landing cases experimentally. The model is based on the physical properties of the F450 and designed FSA, allowing to quantify the effect of each

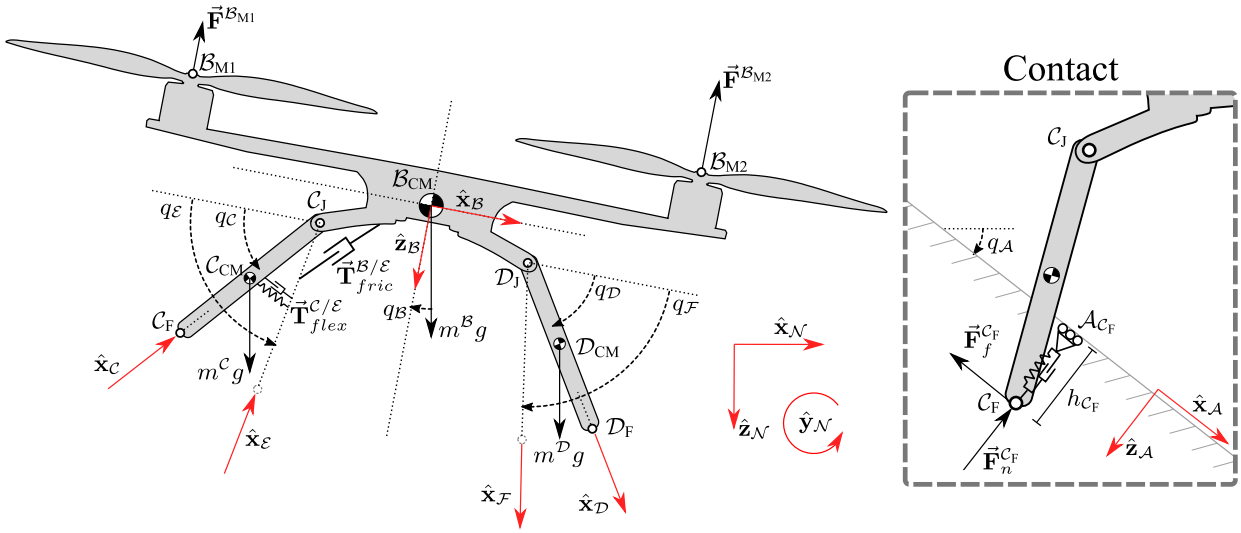

Fig. 4. Diagram of the simplified quadrotor ($\mathcal{B}$), the legs ($\mathcal{C}$ and $\mathcal{D}$) and the surface ($\mathcal{A}$), reference frames and forces included in the dynamic model.

optimization variable discussed in Section II. Assuming the quadrotor is able to align itself before landing, the problem can be simplified to consider the UAV's movement only in a 2D plane (e.g., roll and yaw remain under 10°). The quadrotor model is composed of three rigid bodies: the main body $\mathcal{B}$ and two legs $\mathcal{C}$ and $\mathcal{D}$, as shown in Fig. 4. The position of the quadrotor's center of mass in the inertial frame $\mathcal{N}$ is expressed as $x_{\mathcal{B}}\hat{\mathbf{x}}_{\mathcal{N}} + z_{\mathcal{B}}\hat{\mathbf{z}}_{\mathcal{N}}$, while its pitch rotation is $q_{\mathcal{B}}\hat{\mathbf{y}}_{\mathcal{N}}$. These legs are connected to the main body at joints $\mathcal{C}_\text{J}$ and $\mathcal{D}_\text{J}$. Legs $\mathcal{C}$ and $\mathcal{D}$ are rotated by angles $q_{\mathcal{C}}$ and -$q_{\mathcal{D}}$ respectively, relative to the drone $\mathcal{B}$ about $\hat{\mathbf{y}}_{\mathcal{B}}$.

This section first details the different forces utilized in the model in order to derive the equations of motion. Recorded experimental trials are then used to identify certain unknown parameters of the model.

A. Forces

The various forces modeled are described below.

1) Gravity: The forces of gravity are applied at each body's center of mass ($m^{\mathcal{B}}g$, $m^{\mathcal{C}}g$, $m^{\mathcal{D}}g$).

2) Rotor Thrust: The rotor forces $\vec{\mathbf{F}}^{\mathcal{B}_{\text{M1}}}$ and $\vec{\mathbf{F}}^{\mathcal{B}_{\text{M2}}}$ are applied at points $\mathcal{B}_{\text{M1}}$ and $\mathcal{B}_{\text{M2}}$ respectively in the direction $\hat{\mathbf{z}}_{\mathcal{B}}$. These forces are proportional to the square of the motors' angular velocity, which are obtained through a rotor dynamics model based on Kirchhoff's current law and Newton's second law [15]. This model also includes the startup and reversal delay, as described in [4]. The same rotor parameters and reversing delay are reused.

3) Body Joints: The angular displacement of the legs subjected to friction in the joints are represented by rotations of $q_{\mathcal{E}}\hat{\mathbf{y}}_{\mathcal{B}}$ and -$q_{\mathcal{F}}\hat{\mathbf{y}}_{\mathcal{B}}$. To correctly simulate the quadrotor's landing motion, it was important to consider the legs' and joints' flexibility. Intermediate frames $\mathcal{E}$ and $\mathcal{F}$ were added to model this bending in series with the friction displacement. Torsional spring and damper systems are used to simulate this bending. For example, the spring-damper torque applied on $\mathcal{C}$ by $\mathcal{E}$ is given by

$$\vec{\mathbf{T}}^{\mathcal{C}/\mathcal{E}}_{flex} = (k_q(q_{\mathcal{E}} - q_{\mathcal{C}}) + b_q(\dot{q_{\mathcal{E}}} - \dot{q_{\mathcal{C}}})) \cdot \hat{\mathbf{y}}_{\mathcal{C}}, \tag{2}$$

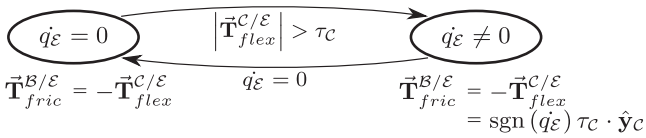

Fig. 5. Equations and transitions for friction torque $\vec{\mathbf{T}}^{\mathcal{B}/\mathcal{E}}_{fric}$, whether frame $\mathcal{E}$ is rotating or not.

where k_q and b_q are, respectively, the spring and the damping constant. The friction torque $\vec{\mathbf{T}}^{\mathcal{B}/\mathcal{E}}_{fric}$ generated at joint $\mathcal{C}_\text{J}$, is applied on $\mathcal{B}$ by $\mathcal{E}$. The kinematics of the massless frames $\mathcal{E}$ and $\mathcal{F}$ are solved before integrating the dynamics of the bodies. To do so, $\mathcal{E}$'s static equilibrium ($\Sigma\vec{\mathbf{M}}^{\mathcal{E}} = 0$) is used to obtain the equations in Fig. 5. In that figure, $\tau_{\mathcal{C}}$ is the level of friction torque in the joint. Depending on the state of the leg, the force balance is solved differently. At the start of the simulation, as the foot $\mathcal{C}_\text{F}$ first hits the ground during the landing, leg $\mathcal{C}$ starts rotating to simulate bending, but frame $\mathcal{E}$ remains immobile ($\dot{q_{\mathcal{E}}} = 0$). Once the bending torque $\left|\vec{\mathbf{T}}^{\mathcal{C}/\mathcal{E}}_{flex}\right|$ is greater than the friction level $\tau_{\mathcal{C}}$, frame $\mathcal{E}$ starts rotating, dissipating kinematic energy through friction. The torque equilibrium allow to solve for $\dot{q_{\mathcal{E}}}$ using (2). Afterwards, $\vec{\mathbf{T}}^{\mathcal{C}/\mathcal{E}}_{flex}$ remains constant until $\dot{q_{\mathcal{E}}}$ returns to 0.

Furthermore, to prevent the landing gears from completely running their course, a separate torsional spring-damper system is activated when $q_{\mathcal{C}}$ and $q_{\mathcal{D}}$ are get within a small angle q_{end} (2°) of the joint limit to rapidly stop the rotation of the leg. A high damping constant of 1 Nm.s/rad was therefore selected to simulate an inelastic impact. Varying the stiffness constant of this spring-damper system did not produce important variations in the simulations as it is in series with the legs' lower compliance.

4) Contact Forces: The normal and friction forces from the contact between the legs and the ground $\mathcal{A}$ are modeled using intermittently activated spring-damper systems and a continuous friction law, as described in [4].

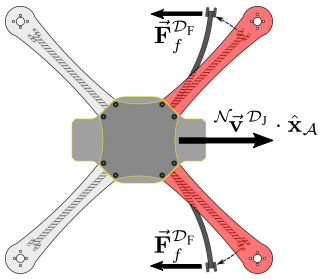

Fig. 6. Top view of a F450, displaying the outwards bending of the legs due to high surface friction.

B. Other Considerations

As observed during the experimental trials, the downhill legs (attached to joint $\mathcal{D}_\mathrm{J}$) of the quadrotor tend to bend backward when the drone is sliding down during landing, as shown in Fig. 6.

This creates two additional phenomenon that need to be considered in order to properly model the drone's dynamics.

1) The friction force on the ground create a moment on the friction joint that increases the total compression forces inside the FSA. This lead to a rise in friction torque of joint $\mathcal{D}_\mathrm{J}$. This can be approximately represented by increasing the friction torque $\tau_\mathcal{D}$ proportionally to the friction force $\vec{\mathbf{F}}_f^{\mathcal{D}_\mathrm{F}}$ between foot $\mathcal{D}_\mathrm{F}$ and the ground with

$$\tau_\mathcal{D} = \tau_{\mathcal{D}input} \left(1 + factor_\tau \cdot \left|\vec{\mathbf{F}}_f^{\mathcal{D}_\mathrm{F}}\right|\right), \qquad (3)$$

where $\tau_{\mathcal{D}input}$ is the expected level of friction torque set into the joint $\mathcal{D}_\mathrm{F}$ and $factor_\tau$ is the proportionality gain that increase the friction torque due to the ground friction force.

2) The friction coefficient of the interface between the foot $\mathcal{D}_\mathrm{F}$ and the ground increases as the foot's rubber catches more easily into the surface's asperities as the legs bend outward. This phenomenon is less prominent on the uphill legs as they bend inward when loaded. It is approximated by increasing the downhill foots' friction coefficient proportionally to the velocity of joint $\mathcal{D}_\mathrm{J}$ in the $\hat{\mathbf{x}}_\mathcal{A}$ direction with

$$\mu_{k\mathcal{D}} = \mu_k \left(1 + factor_{\mu_k} \left(^{\mathcal{N}}\vec{\mathbf{v}}^{\mathcal{D}_\mathrm{J}} \cdot \hat{\mathbf{x}}_\mathcal{A}\right)\right), \qquad (4)$$

where μ_k is the base kinetic friction coefficient and $factor_{\mu_k}$ is the proportionality factor.

C. Equations of Motion (EOM)

The system's EOM are obtained by solving for the system's states ($x_\mathcal{B}$, $z_\mathcal{B}$, $q_\mathcal{B}$, $q_\mathcal{C}$ and $q_\mathcal{D}$) and their time-derivative, as well as the unknown linkage forces connecting both legs to the main body of the quadrotor. A Newton-Euler approach was used to derive the EOM. Scalar equations can be obtained by extracting the $\hat{\mathbf{x}}_\mathcal{N}$ and $\hat{\mathbf{z}}_\mathcal{N}$ components for linear motion and the $\hat{\mathbf{y}}_\mathcal{N}$ component for angular motion. The EOM were derived using MotionGenesis [16] and solved in Matlab.

TABLE II
DJI F450 AND FSA PHYSICAL PARAMETERS

Parameter	Measured	GA mean ($\bar{x} \pm \sigma$)
$m^\mathcal{B}$ (kg)	1.502	—
$I_{yy}^{\mathcal{B}/\mathcal{B}_\mathrm{CM}}$ (kg.m^2)	0.0138	—
$m^\mathcal{C}$ (kg)	0.029	—
$I_{yy}^{\mathcal{C}/\mathcal{C}_\mathrm{CM}}$ (kg.m^2)	9.8e-5	—
k_q (N.m/rad)	—	16.4±0.78
b_q (N.m.s/rad)	—	0.085±0.017
k_g (N/m) [a]	—	2.17e4±7.77e3
b_g (N.s/m) [a]	—	437±72
μ_k	—	0.80±0.023
$factor_\tau$	—	5.8e-4±5.6e-4
$factor_{\mu_k}$	—	0.57±0.02

[a] Coefficients of the spring-damper system modeling feet contact with the ground

D. Parameter Identification and Validation

For the proposed model to accurately predict the outcome of a quadrotor landing, the parameters listed in Table II had to be identified. Similar to previous work [4], an unpowered DJI F450 equipped with the FSA joints was dropped a total of 10 times on a surface covered by roofing shingles at inclinations varying between 0° and 45°, and at vertical velocities ranging from 1 to 3 m/s. These drops were recorded using a motion tracking system at 200 Hz. For each drop, different friction torques were set in the joint, in some cases to favor a successful landing and in others to purposely flip over the quadrotor. These friction torques were measured with a dynamometer. The mass of each body were measured. The moment of inertia was measured using a bifilar pendulum [17].

Genetic algorithms (GA) were then used to fit the model to these recorded drops by identifying the seven unknown parameters from Table II. Three identical GAs were conducted with different sets of six drops from the 10 recorded drops. The GAs were used to minimize the average normalised root-mean-squared error (NRMSE) between six measured and simulated states ($x_\mathcal{B}$, $z_\mathcal{B}$, $q_\mathcal{B}$, $\dot{x}_\mathcal{B}$, $\dot{z}_\mathcal{B}$ and $\dot{q}_\mathcal{B}$) over the six drops. The weight of the angular states were twice those of the linear states. The GAs were set in Matlab using a population of 1000 individuals and were set to end when the NRMSE change over 4 generations was less 0.02%. The GAs yielded three slightly different sets of parameters with NRMSE ranging between 13.1% and 13.5% (average over the six drops). The four unused recorded drops per GA were used to validate these discovered sets of parameters. The NRMSE obtained from these validation sets ranged between 15.1% and 18.6%, confirming that the parameters don't overfit the model. An example of the comparison between an experimental drop and its simulated counterpart is presented at Fig. 7.

Each GA was able to correctly predict if the drone would flip over or not, in both training and validation sets. These results confirm the model's accuracy to predict the quadrotor dynamics and the outcome of a given landing scenario.

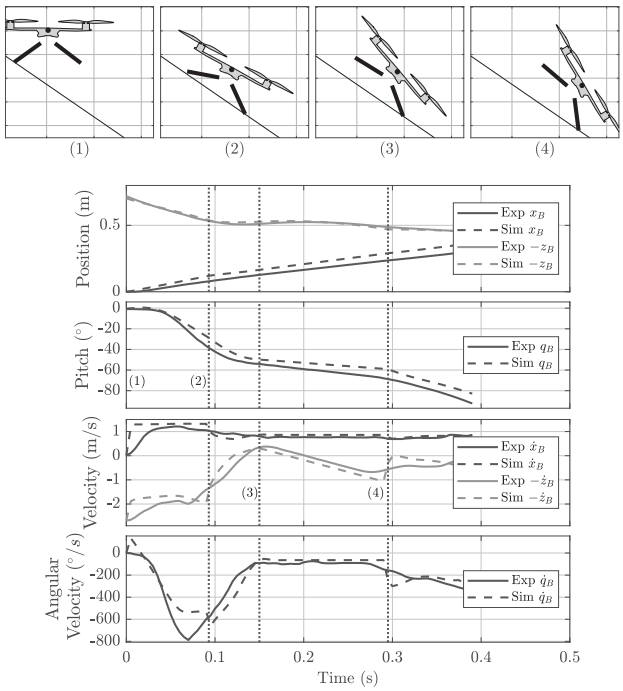

Fig. 7. UAV position (x_B, z_B), pitch (q_B), velocity ($\dot{x_B}$, $\dot{z_B}$) and angular velocity ($\dot{q_B}$) during an experimental and simulated landing on roofing shingles (bottom), and simulated visual of four instances near the start of the drop (top). The drop was performed on an inclination of 35° at a vertical impact speed of 2.7 m/s. In this training case, the simulation used the parameters from the 2nd GA and yielded an NRMSE of 11.2%. At the moment of impact (1), the friction joint starts compressing and the drone rotates. The downhill leg impact slows the rotation down as well as the vertical velocity (2). The hard impact combined with leg flexibility causes the drone to bounce upwards while still rotating (3). Finally, the F450 lands on its downhill legs, and the friction causes the drone to flip over (4).

V. Results

Using the validated model allows to quickly explore the design space of the landing gear and the effects of modifying the landing optimization variables.

A. Symmetric Friction Torque

Maps can be generated to observe the landing envelope as a function of vertical impact velocity and surface inclination. Fig. 8 shows the outcome of landings when both τ_C and τ_D are equal to 1.7 Nm. These simulations did not include any thrust. The green area on the map represents conditions which resulted in an ideal successful landing, where the landing gears were well used to dampen the impact. The blue area also corresponds to successful landings, however the FSAs were not compressed by more than 40%, indicating that the friction level was too high and were not as useful as they could have been. The orange area indicates when one of the FSAs completely ran its course and reached its EOT. This could potentially lead to harder impacts and damages. The white zone indicates that the quadrotor has slid further than 1 m down the slope or was still in motion after 2 s of simulation, which can occur at low speeds on high inclinations. The light and dark gray respectively represent conditions where one of the joints hits the surface and where the drone flips over (reaches a pitch angle of less than −80°),

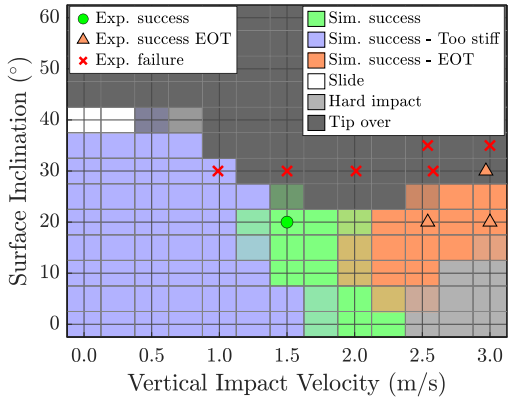

Fig. 8. Simulated landing envelope when using friction torques $\tau_C = \tau_D = 1.7$ Nm. Results from experimental trials are added. Green circles represent successful landings, orange triangles represent successful landings but with the landing gear reaching its end of travel, and red crosses are failures.

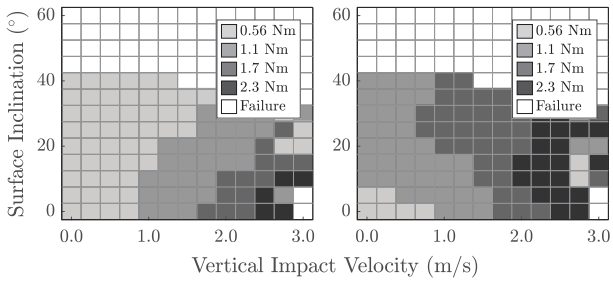

Fig. 9. Ideal uphill friction torque τ_C (left) and downhill friction torque τ_D (right) that yield optimal probability of successful landing for each impact condition.

both of which present a high risk of damaging the UAV. The map was simulated three times using the three sets of physical parameters obtained by the GAs, which explained the gradient of color between each distinct zone as the outcome is slightly different for each set of parameters.

Without implementing leg flexibility in the model, the landing predictions were highly optimistic when compared to experimental results. Indeed, leg compliance reduces the landing performance by storing and releasing energy, which can contribute to the UAV flipping. Future designs could benefit from increased leg structural stiffness.

B. Asymmetric Friction Torque

For every landing condition of the map, landings were simulated using different combinations of τ_C and τ_D (0.56, 1.1, 1.7 and 2.3 Nm). The best combination is the one where the shock absorbers compressed the most without reaching their EOT. Fig. 9 illustrates the optimal combination of friction torque. Using these torque levels, the envelope reaches 35°–40° inclinations over the full vertical velocity range considered.

C. Asymmetric Leg Orientation

As mentioned in Section II, decreasing the initial angle q_C of the uphill leg allows the quadrotor to land on steeper inclines by encouraging joint motion. On horizontal surfaces, both q_C and q_D are set at their maximum (37.5°). It was found empirically that

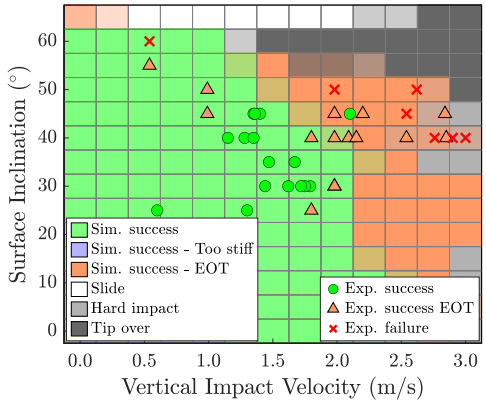

Fig. 10. Simulated landing envelope using asymmetric friction torque and leg orientation as well as RVT. Indoor (25 to 60°, 0.5 to 3 m/s) and outdoor (25 to 45°, 1.5 to 3 m/s) experimental landings are included.

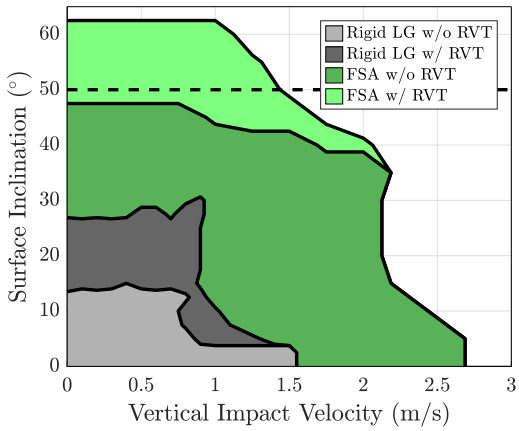

Fig. 11. Simulated landing envelopes for a traditional F450 with rigid landing gear (LG) with and without RVT [4], and for a F450 equipped with FSAs (FSA) with optimal asymmetric friction torques leg orientation, with and without RVT. Only the green zones are portrayed in this envelope. The static friction limit of the F450 on a shingled surface is represented by the dotted line.

q_C should decrease linearly to 24° for inclines of 40°. Landing performances for these conditions are shown in dark green in Fig. 11. Using asymmetric leg orientation, the UAV is capable of landing on surface inclinations of up to 50°.

D. Reverse Thrust

Varying friction torque and leg orientation allows the F450 to land on inclinations approaching its static friction limit of 50°. Beyond that limit, the drone slides or bounces down the slope. RVT can be used to increase the maximum allowable inclination. Simulations were conducted with 100% RVT commanded at the moment of impact. The landing envelope generated using this approach is presented in Fig. 10. The envelope is significantly increased, allowing landings on inclinations of 60°, beyond the friction limit of the drone. Low power adhesion mechanisms, such as switchable magnets, grippers or dry-adhesives, could be used to remain on the surface after terminating RVT. One can note the larger orange zones, which are due to the uphill FSA reaching its EOT because of the combination of its reduced initial angle and friction torque with high velocity impact. Experimental trials, shown in Fig. 10, were also conducted to validate the

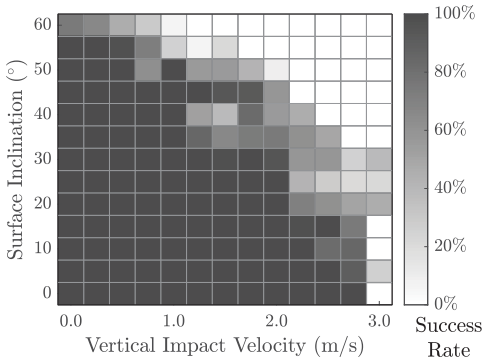

Fig. 12. Success rate for landings (with $-10° \leq q_B \leq 10°$ and $-60°/s \leq \dot{q}_B \leq 60°/s$) using best friction torque combination for level landing.

simulated envelope. These results show that the model is slightly optimistic at higher angles, which is mostly due to not having used drops on inclinations above 45° in the GAs.

Finally, using data from previous work [4], Fig. 11 demonstrates the performance gain that provides the FSAs, with and without reverse thrust, compared the traditional rigid landing gear of an F450 quadrotor. The envelope granted by the proposed design and RVT is 8 times larger than the one of a stock F450.

E. Robustness

Although the suspension can be adjusted to optimize the chance of success for specific conditions, one advantage of this suspension is its robustness to the exact landing conditions. As shown in Fig. 8, a set friction torque level combination allows the UAV to land on in a wide range of impact velocities and surface angles.

All previous simulations begin with the drone at level attitude. To further demonstrate the robustness of the proposed landing strategy, thousands of simulations were conducted with non-ideal attitude at impact, i.e., using q_B between $-10°$ and 10°, $\dot{q}_B$ between -60 and 60°/s. By using the optimal friction torque levels previously determined for each speed and surface angle, it was found that the rate of success remains 81% of the landing envelope illustrated in Fig 10. Detailed results from these simulations are presented in Fig. 12.

VI. Experimental Validation

The landing gear was put to test in outdoor situations. These trials validated the robustness of the landing system previously simulated to realistics landing conditions. Limited on-board sensors (rangefinder and GPS) and wind gusts complicated the task of manoeuvring and orienting the drone perfectly over the small landing zone and landing in a straight line. Therefore, outdoor testing will give a true sense of the system's landing capabilities.

A. Software Implementation

The Ardupilot firmware was modified to incorporate a landing state-machine to perform outdoor trials using the landing gear and RVT. Once the pilot has directed the UAV above the landing zone with its heading roughly facing the slope, the landing sequence is manually engaged. Then, the quadrotor descends

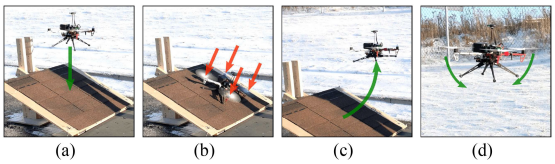

Fig. 13. Sequence example for landing on an inclined roof, starting with the descent (a), impact and activation of RVT (b), takeoff (c) and reset of leg orientation (d).

at a rate of 0.5 m/s while the rangefinder is used to detect the ground. The motors are turned off at 30 cm above the surface. The IMU is then used to detect impact and start the RVT.

The system allows the pilot to perform multiple consecutive landings by controlling the friction in the legs with joystick commands. After a first landing, the pilot takes off and reduces the friction in the joints to allow the springs to bring the legs back to their initial position. The pilot then reactivates the desired friction level based on the next landing. This sequence was performed outdoors multiple times, as shown in Fig. 13.

B. Results

A total of 25 different landings were performed at various angles ranging from 25 to 45° and touchdown speeds ranging from 1.5 to 3 m/s. These trials are also presented in Fig. 10. To further evaluate robustness, the optimal friction torque and leg orientations were not always perfectly set for each specific landing. Nevertheless, the system demonstrated its ability to land on each of the 25 trials. The system showed great landing capabilities and robustness to external perturbations, even with basic sensors. In fact, during those 25 trials, the heading angle and horizontal speed varied respectively in the range of $\pm 10°$ and ± 0.4 m/s at impact. Considering the average residential roof slopes in North America are typically between 4:12 (18°) and 9:12 (37°) [18], the UAV developed could easily land on most Canadian roofs, either to save energy, recharge or observe its surroundings.

VII. Conclusion

This paper evaluates the effectiveness of using friction as a means to dissipate a quadrotor's kinetic energy during high velocity impacts on inclined surfaces. The proposed landing gear design, weighing only 320 g, enables an F450 drone to more than double its vertical impact velocities and nearly quadruple its maximum allowable inclination at landing, resulting in an increase of the landing envelope by a factor of 8. When combined with RVT, the maximum inclination is further increased to 60°, above the friction limit of the drone with the surface. In the current implementation, the friction level of each FSA can be modulated before impact to provide the best chances of success depending on the expected landing conditions. This approach is robust, as impact conditions are not limited to level landings and do not require to be precisely known before impact. Experimental trials confirm the FSA's performance and the designed model can be used to explore further landing scenarios.

Future work will include more extensive trials of the proposed solution in complex landing situations (high winds, rocky inclined terrain, rocking ships and fast moving vehicles). The weight of the landing gear could be further decreased using other materials such as carbon fiber. This would also increase its rigidity to reduce the negative effects related to the bending of the legs. Other friction mechanisms, like magnetorheological clutches [19], could also provide rapid modulation of friction levels.

References

[1] K. W. Williams, "A summary of unmanned aircraft accident/incident data: Human factors implications" US Department of Transportation FAA Civil Aerospace Medical Institute, Oklahoma City, USA, Tech. Rep. DOT/FAA/AM-04/24, 2004.

[2] D. Hentzen, T. Stastny, R. Siegwart, and R. Brockers, "Disturbance estimation and rejection for high-precision multirotor position control," in *Proc. IEEE Int. Conf. Intell. Robots Syst*, 2019, pp. 2797–2804.

[3] E. Atkins and J. Castagno, "Rooftop landings for safe urban drone operations," presented at the Amazon re:MARS., Las Vegas, NV, USA, 2019.

[4] J. Bass and A. L. Desbiens, "Improving multirotor landing performance on inclined surfaces using reverse thrust," *IEEE Robot. Automat. Lett.*, vol. 5, no. 4, pp. 5850–5857, Oct. 2020.

[5] J. Thomas *et al.*, "Aggressive flight with quadrotors for perching on inclined surfaces," *J. Mechanisms Robot.*, vol. 8, no. 5, 2016, Art. no. 051007.

[6] D. Mehanovic *et al.*, "Autonomous thrust-assisted perching of a fixed-wing UAV on vertical surfaces," in *Proc. Conf. Biomimetic Biohybrid Syst.*, 2017, pp. 302–314.

[7] D. Brescianini and R. D'Andrea, "Design, modeling and control of an omni-directional aerial vehicle," in *Proc. IEEE Int. Conf. Robot. Autom.*, 2016, pp. 3261–3266.

[8] F. von Frankenberg and S. B. Nokleby, "Inclined landing testing of an omni-directional unmanned aerial vehicle," *Trans. Can. Soc. Mech. Eng.*, vol. 42, no. 1. pp. 61–70, 2018.

[9] C. Luo, X. Li, Y. Li, and Q. Dai, "Biomimetic design for unmanned aerial vehicle safe landing in hazardous terrain," *IEEE/ASME Trans. Mechatronics*, vol. 21, no. 1, pp. 531–541, Feb. 2016.

[10] J. Liu *et al.*, "A multi-finger robot system for adaptive landing gear and aerial manipulation," *Robot. Auton. Syst.*, vol. 146, 2021, Art. no. 103878.

[11] M. Ikura *et al.*, "Stabilization system for uav landing on rough ground by adaptive 3D sensing and high-speed landing gear adjustment," *J. Robot. Mechatronics*, vol. 33, no. 1, pp. 108–118, 2021.

[12] K. Zhang *et al.*, "Bioinspired design of a landing system with soft shock absorbers for autonomous aerial robots," *J. Field Robot.*, vol. 36, no. 1, pp. 230–251, 2019.

[13] J. Dixon, *The Shock Absorber Handbook*, Hoboken, NJ, USA: Wiley, 2008.

[14] D. Baker and W. Haynes, "Disc friction," 2018. [Online]. Available: https://engineeringstatics.org/Chapter_09-disc-friction.html

[15] W. Khan and M. Nahon, "Toward an accurate physics-based UAV thruster model," *IEEE/ASME Trans. Mechatronics*, vol. 18, no. 4, pp. 1269–1279, Aug. 2013.

[16] P. Mitiguy, *Advanced Dynamics and Motion Simulation*, Sunnyvale, CA, USA: Prodigy Press, 2014.

[17] M. P. Miller, *An Accurate Method of Measuring the Moments of Inertia of Airplanes*. vol. 351, Washington, DC, USA, Nat. Advisory Committee Aeronaut., 1930.

[18] IKO, "What is the minimum slope for an asphalt shingle roof," 2022. [Online]. Available: https://www.iko.com/na/pro/building-professional-tools/roofing-101/minimum-slope-for-asphalt-shingle-roof/

[19] L.-P. Lebel, J.-A. Verreault, J.-P. L. Bigué, J.-S. Plante, and A. Girard, "Performance study of low inertia magnetorheological actuators for kinesthetic haptic devices," in *Proc. IEEE World Haptics Conf.*, 2021, pp. 103–108.